



Cite this: DOI: 10.1039/c9tc00051h

Luminescent switching and structural transition through multiple external stimuli based on organic molecular polymorphs†

Bo Shao,^{‡a} Rihua Jin,^{‡b} Aisen Li,^a Yingjie Liu,^a Bao Li,^{id a} Shuping Xu,^{id *a}
Weiqing Xu,^{id a} Bin Xu^a and Wenjing Tian^{id *a}

Investigations on the relationship between multi-stimuli responsive luminescent properties and aggregation structures of polymorphs play a crucial role in developing organic multi-stimuli responsive luminescent (OMSRL) materials. Herein, we reported two polymorphs (G-phase and O-phase) based on a novel molecule 9,10-bis-((E)-4-(pyridin-3-yl)styryl)anthracene (**BP3SA**) and their piezochromic properties, structural transitions, and protonation–deprotonation effects under external stimuli. Photophysical characterization together with the analysis of crystal structures indicated that the G-phase with J-type aggregation showed green emission, while the O-phase with H-type aggregation presented orange emission. Red-shifted emissions could be observed for the two polymorphs under mechanical grinding pressure due to the transition from the crystalline state to the amorphous state. Then upon heating, the ground G-phase could partly recover the initial emission, while the emission of the ground O-phase nearly turned to the initial emission of the G-phase after heating. Powder X-ray diffraction patterns revealed that a structural transition from the O-phase to the G-phase could be achieved by grinding and heating processes. High pressure experiments and theoretical calculations demonstrated that the O-phase showed a more significant red-shift than the G-phase, and the molecular geometry of the O-phase trended toward a more planar conformation than that of the G-phase under the same hydrostatic pressure. It indicated that the O-phase had higher sensitivity to the hydrostatic pressure than the G-phase because of the different intermolecular interactions inside the two crystalline phases. Additionally, the protonation–deprotonation of the two polymorphs showed that acid stimuli could induce red-shifted emission, while the emission partly recovered to the initial emission by alkali stimuli due to the change of the intermolecular interactions.

Received 4th January 2019,
Accepted 13th February 2019

DOI: 10.1039/c9tc00051h

rsc.li/materials-c

Introduction

Organic luminescent materials have attracted more and more attention due to their unique electronic structure and optical properties.¹ Organic multi-stimuli responsive luminescence (OMSRL) materials are of great importance because of their structural tunability and widespread applications in the fields of optoelectronics, such as sensors,² switches,³ memories⁴ and so on. As organic molecular luminescent crystals have definite conformation and packing mode, this can provide a visualized model to precisely investigate the relationship between the

aggregate structure and luminescent properties.⁵ Great effort has been devoted to the research on organic molecular luminescent crystals and their multi-stimuli responsive luminescent properties. For example, piezochromic luminescent materials based on twisted molecular structures, such as tetraphenylethylene,^{4,6} divinylanthracene,^{5b,7} triphenylamine⁸ and boron-containing compounds⁹ and other compounds,¹⁰ have been investigated through the manipulation of molecular packing modes/intermolecular interactions by grinding or hydrostatic pressure treatments. Moreover, acid-dependent luminescent materials containing an alkaline group, such as pyridine,^{6c,7a,11} diazine,¹² piperidine,¹³ and other groups,¹⁴ have also been studied by changing their conformations or frontier molecular orbitals with acid.

Based on the research around the multi-stimuli responsive properties of 9,10-bis((E)-2-(pyridin-3-yl)viny)anthracene (**BP3VA**)^{11b} in our group, we designed and synthesized a novel molecule 9,10-bis-((E)-4-(pyridin-3-yl)styryl)anthracene (**BP3SA**) by introducing benzyl groups into **BP3VA**. Two polymorphs (G-phase and O-phase)

^a State Key Laboratory of Supramolecular Structure and Materials, Jilin University, Changchun 130012, P. R. China. E-mail: wjtian@jlu.edu.cn, xusp@jlu.edu.cn

^b Department of Neurosurgery, The First Hospital of Jilin University, Changchun 130012, P. R. China

† Electronic supplementary information (ESI) available. CCDC 1581638–1581640. For ESI and crystallographic data in CIF or other electronic format see DOI: 10.1039/c9tc00051h

‡ Two authors have equal contribution for this manuscript.

based on BP3SA were obtained by using a solvent evaporation method. Piezochromic properties, structural transitions, together with the protonation–deprotonation effect were investigated for the two polymorphs. The luminescent switching and structural transition can be realized by grinding and further heating processes. High pressure experiments together with the theoretical calculation reveal that the O-phase is more sensitive to the hydrostatic pressure than the G-phase because of the fewer interactions among the adjacent molecules in the O-phase. In addition, the protonation–deprotonation of the pyridine moieties has a significant effect on the destruction of various C–H...N bonds in the G-phase, resulting in more distinct luminescent switching of the G-phase than that of the O-phase under acid and alkali stimuli.

Experimental section

Materials and methods

All starting materials were purchased by commercial approaches and used without further purification. THF was dried by distillation from sodium/benzophenone under nitrogen.

¹H NMR spectra were obtained using a Bruker AVANCE 500 MHz spectrometer. UV-vis absorption spectra were recorded by using a Shimadzu UV-3100 spectrophotometer. Photoluminescence spectra were collected with a Shimadzu RF-5301PC spectrophotometer and a Maya 2000Pro. optical fibre spectrophotometer. Solid-state PL efficiencies were measured by means of an integrating sphere12 (C-701, Labsphere Inc.), with a 365 nm Ocean Optics LLS-LED as the excitation source. The excitation light was introduced into the sphere through an optical fibre.

Synthesis

BP3SA was synthesized by using the procedure shown in Scheme S1 (ESI[†]) and characterized by ¹H NMR, and mass spectroscopies.

Compound 1 (9,10-bis(chloromethyl)anthracene) and compound 2 (tetraethyl anthracene-9,10-diylbis(methylene)diphosphonate) were synthesized according to the previously reported methods. Compound 2 (1.435 g, 3.00 mmol) was stirred with 4-bromobenzaldehyde (2.755 g, 14.89 mmol) in THF (90 mL) under nitrogen. *t*-BuOK (1.346 g, 11.20 mmol) in THF (60 mL) was added dropwise to the solution, and then the mixture was stirred for 12 h at 50 °C. After removing the solvent (THF), the resulting precipitate was filtered, washed by methanol and purified by column chromatography using dichloromethane and petroleum ether. Compound 3 (0.871 g) was obtained in a yield of 54%. ¹H NMR (500 MHz, CDCl₃) δ 8.37–8.35 (m, 4H), 7.93 (d, *J* = 20.0 Hz, 2H), 7.57 (q, *J* = 8.5 Hz, 8H), 7.50–7.19 (m, 4H), 6.88 (d, *J* = 15.0 Hz, 2H).

Compound 3 (270.10 mg, 0.50 mmol), 3-pyridineboronic acid pinacol ester (256.33 mg, 1.15 mmol), Pd(PPh₃)₄ (34.67 mg, 0.03 mmol) and 2 M Na₂CO₃ (8.3 mL) were stirred with back-flow in THF (12.3 mL) under nitrogen at 65 °C for 24 h. The mixture was cooled to ambient temperature. After removing the solvent, the resulting precipitate was dissolved with CH₂Cl₂, and extracted with H₂O. The organic phase was concentrated

and purified by column chromatography using dichloromethane and methanol (100 : 1) to get a yellow powder with a yield of about 88%. ¹H NMR (500 MHz, CDCl₃) δ 8.96 (s, 2H), 8.65 (d, *J* = 4.0 Hz, 2H), 8.43–8.41 (m, 4H), 8.09–8.00 (m, 4H), 7.83 (d, *J* = 8.5 Hz, 4H), 7.71 (d, *J* = 8.0 Hz, 4H), 7.53–7.49 (m, 6H), 7.00 (s, 1H), 7.03 (s, 1H). MS *m/z*: calcd for C₄₀H₂₈N₂: 536.23; found 536.03.

Single-crystal X-ray crystallography studies

Crystal diffraction data were obtained with graphite-monochromated Mo/Cu Kα radiation using a Rigaku RAXISRAPID diffractometer. The structure was solved by the direct method using the SHELX program and refined with least-squares methods. Anisotropic thermal parameters were refined for all of the non-hydrogen atoms. Hydrogen atoms were added at the idealized positions and refined using isotropic displacement.

Diamond anvil cell technique

Hydrostatic pressure was obtained from a diamond anvil cell (DAC) (BGI-type DAC) with 400 μm culet diamonds. A 0.25 mm thick T301 stainless steel gasket (*d* = 5.00 mm) was drilled to make a hole with a diameter of 0.2 mm as the sample chamber. G-Phase crystal and O-phase crystal were placed in the sample chamber, and a small ruby chip was introduced into the same hole for *in situ* pressure calibration according to the fluorescence shift of the ruby R1 line. And then, silicone oil was added as a pressure-transmitting medium (PTM), which can provide a guarantee for obtaining the hydrostatic pressure according to Pascal's principle. The high-pressure fluorescence spectra under hydrostatic conditions were measured using a fluorescence microscope (IX71, Olympus, 50×, NA = 0.5) equipped with a spectrometer (Jobin Yvon iHR320). The light source was a mercury lamp with an excitation wavelength of 365 nm.

DFT calculations at GGA-PBE level under different external stress

The single crystal DFT calculations under different applied pressures were performed by means of the CASTEP module in Material Studio. The exchange–correlation (XC) effects were described by utilizing the generalized gradient approximation (GGA) with Perdew–Burke–Ernzerhof (PBE). A TS scheme was used for dispersion corrections. This calculation was done with a plane wave set using norm-conserving pseudopotentials with 750 eV energy cut off. For geometry optimization, the energy tolerance was 2.0 × 10^{−5} eV per atom with a force tolerance of 0.05 eV Å^{−1}, a maximum displacement of 2.0 × 10^{−3} Å, and a maximum stress tolerance of 0.10 GPa. For the self-consistent field (SCF) calculation, the energy tolerance was set to 1.0 × 10^{−6} eV per atom.

Results and discussion

Crystal structures

Single crystals have a highly ordered molecular packing structure that makes them the ideal model to investigate the relationship between the aggregation structure and luminescence properties.

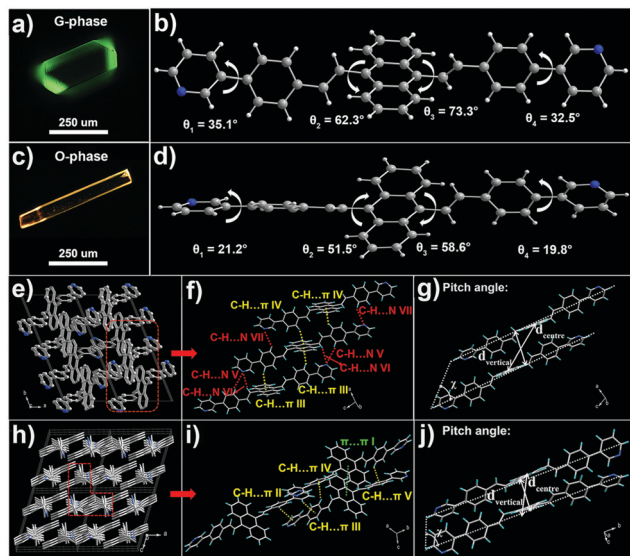


Fig. 1 Images and molecular conformation of G-phase (a and b), O-phase (c and d). (e) The perspective view of G-phase cells along the *c*-axis. (f) The intermolecular interactions between adjacent molecules in G-phase. (g) The vertical distance, the centre distance and the pitch angle in G-phase. (h) The perspective view of O-phase cells along the *b*-axis. (i) The intermolecular interactions between adjacent molecules in O-phase. (j) The vertical distance, the centre distance and the pitch angle in O-phase.

By solvent evaporation in a dichloromethane solution, the G-phase and O-phase suited for X-ray structural analysis were obtained. Through the analysis of the two crystals, we found that the molecular conformations of the G-phase maintained larger torsion angles θ (Fig. 1b), and the packing structures of the G-phase and O-phase were totally different from each other.

G-Phase crystals were triclinic, and the space group was $P\bar{1}$. As shown in Fig. 1f and Fig. S4 (ESI[†]), the main interactions between the adjacent molecules in G-phase crystals were C–H \cdots π and C–H \cdots N interactions (for detailed data see Table S2, ESI[†]). Along the *b* axis, the phenyl moiety along the long axis of one molecule acted as the H donor and the corresponding anthracene core of an adjacent molecule acted as the acceptor. In C–H \cdots N interactions, the phenyl and vinyl moieties acted as the H donor, and the pyridyl moiety of the adjacent molecule acted as the H acceptor. For the G-phase, the molecules adopted a stacking mode with J-type aggregation along the *b* axis (Fig. 1g, $\chi = 39.5^\circ$) and there was no overlap between the central anthracene planes, indicating that no $\pi\cdots\pi$ interactions were formed in the G-phase ($d_{\text{centre}} = 9.84 \text{ \AA}$, and $d_{\text{vertical}} = 3.14 \text{ \AA}$ between the adjacent molecules).

O-Phase crystals belonged to the monoclinic system, $P2_1/c$ space group with the molecules adopting a stacking mode similar to the H-type aggregation along the *c* axis (Fig. 1j, $\chi = 73.3^\circ$).¹⁵ In Fig. 1i, each molecule interacted with the adjacent molecule *via* $\pi\cdots\pi$ and C–H \cdots π interactions (for detailed data see Table S3, ESI[†]). The adjacent anthracene planes overlapped with other molecules by around 30%. The centre distance d_{centre} between two molecules in the O-phase was measured to be 4.8 \AA , and the vertical distance d_{vertical} between two anthracene planes was

measured to be 3.7 \AA , as shown in Fig. 1j. Thus, owing to the large overlap and short distance between the adjacent anthracene planes, there was relatively strong $\pi\cdots\pi$ stacking.^{7a}

Photophysical properties

The photophysical properties of **BP3SA** were investigated in THF solution and the solid state. As shown in Fig. 2a, the maximum absorption of **BP3SA** in THF solution appeared at 417 nm, and the corresponding emission spectrum exhibited a peak at 638 nm. A large Stokes shift ($4.43 \times 10^4 \text{ cm}^{-1}$) and low photoluminescence quantum yield (PLQY) (0.19 of **BP3SA**) were observed in solution. When the molecules were in the solid state form, the luminescence intensity shows a sharp increase. The maximum absorption of the pristine **BP3SA** powder appeared at 433 nm, and the emission spectrum exhibited a peak at 509 nm and PLQY up to 0.55. In a crystalline state, both crystals possessed high PLQY which were 0.98 for G-phase and 0.48 for O-phase, respectively. Additionally, the two crystalline phases showed a red-shifted emission from 511 nm to 575 nm and a decrease in PLQY from the G-phase to the O-phase (Fig. 2b), which could be understood through their packing structures from J-type to H-type aggregation. Meanwhile, the theoretical study shown in Fig. S9 (ESI[†]) also indicated that the highest occupied molecular orbital (HOMO) and the lowest unoccupied molecular orbital (LUMO) of the O-phase were delocalized a little more, stabilizing the molecules in the excited states and giving rise to the decrease in the band gap (Fig. S9, ESI[†]). Thus, the O-phase had a smaller band gap 3.15 eV, which could be in accordance with the shift of the PL spectrum to a longer wavelength.

Piezochromic behavior

As shown in Fig. 3a, a dramatic luminescence change $\Delta\lambda = 68 \text{ nm}$ in the G-phase was observed after grinding along with the colour change from green (511 nm) to orange (579 nm), and it recovered to yellow green (544 nm) by heating at $150 \text{ }^\circ\text{C}$ for 5 min. In Fig. 3b, the luminescence change $\Delta\lambda = 3 \text{ nm}$ from 575 to 578 nm was shown after grinding the O-phase. Different from the result of heating of the ground G-phase powder, the emission of the O-phase shifted to 538 nm, after being heated under the same condition. These results suggested that the aggregation structure was changed during the grinding and heating process, contributing to the structural transition.

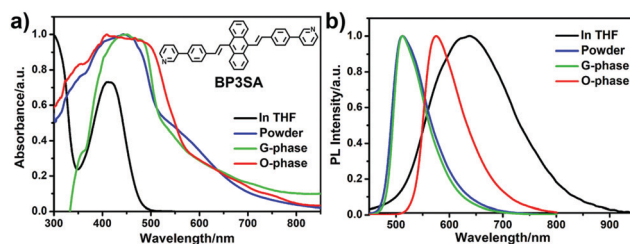


Fig. 2 UV-vis spectra (a) and PL spectra (b) of **BP3SA** in THF, powder, G-phase and O-phase. The excitation wavelength is 365 nm. (Inset: The molecular structure of **BP3SA**.)

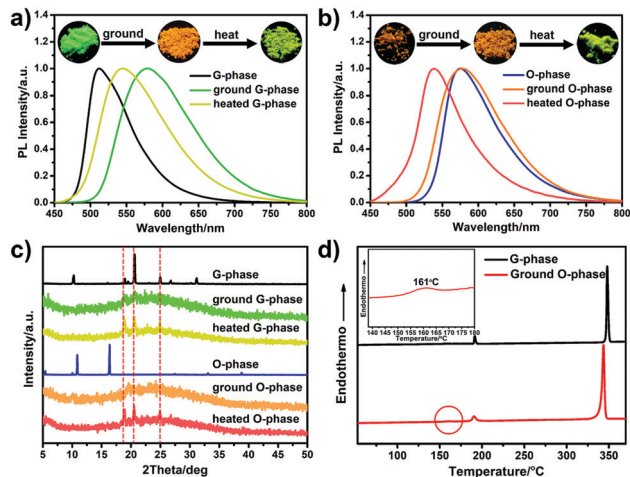


Fig. 3 (a and b) PL spectra of G-phase and O-phase upon different treatments with excitation at 365 nm (inset: images of G-phase and O-phase upon different treatments). (c) PXRD patterns of G-phase and O-phase upon different treatments. (d) DSC patterns of G-phase and ground O-phase.

In order to understand the structural transition between the G-phase and O-phase, PXRD of the two crystals under different treatments was performed. The diffraction patterns of the ground G-phase and O-phase exhibited a wide swell, indicating that the initial aggregation state was changed by grinding, from different crystalline states to amorphous states. After heating, the diffraction patterns of the two samples showed the same three sharp and intense reflections which were consistent with the PXRD pattern of the G-phase. Moreover, the differential scanning calorimetry (DSC) measurements of the G-phase and ground O-phase were performed, as shown in Fig. 3d. Both the G-phase and ground O-phase exhibited two identical peaks at 190 °C and around 345 °C, but an extra endothermic peak at 161 °C could be clearly observed in the ground O-phase, indicating that the ground O-phase exhibited a metastable amorphous phase and converted to a stable G-phase *via* an endothermic process.¹⁶ It suggested that the crystal structures of BP3SA could be readily influenced and transformed by the external stimuli.

In order to further understand the piezochromic behaviour of the two crystals, the effect of hydrostatic pressure on the luminescence of BP3SA was investigated. As shown in Fig. 4, as the applied pressure increased, the luminescence emissions of the G-phase and O-phase had gradual red-shifts. For the G-phase, the emission changed from green (511 nm) to deep red (660 nm) when the pressure increased from 0 to 5.27 GPa. As for the O-phase, the emission colour changed from orange (575 nm) to red (641 nm) with the increase in the pressure from 0 to 2.02 GPa. When the pressure turned back to 0 GPa, the emission of the G-phase partially recovered to the original state. But that of the O-phase recovered to the original state completely, indicating its good reversibility under the pressure stimulus. In order to understand the different sensitivities of the G-phase and O-phase, we calculated the ratio of the wavelength and pressure by the following equation: $k = \frac{\lambda_1 - \lambda_2}{p_1 - p_2}$ (k represents the sensitivity,

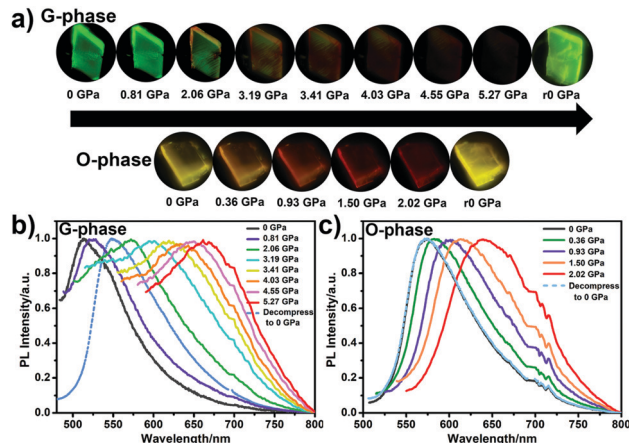


Fig. 4 (a) Images of G-phase and O-phase under different applied pressures ('r0' represents 'release pressure to 0'). (b and c) PL spectra of G-phase and O-phase under different applied pressures. The excitation wavelength is 365 nm.

and λ_1 and λ_2 refer to the maximum emission-peak wavelengths at pressures of p_1 and p_2 , respectively).^{6e} The k value of the G-phase was calculated to be 29.1 nm GPa⁻¹ at around 2.0 GPa, while the k value of the O-phase was 33.2 nm GPa⁻¹, which indicated a better sensitivity of the O-phase to the pressure.¹⁷ On the other hand, the origin of different sensitivities could be understood from the intermolecular interactions in the crystal structure. The various intense C-H...N interactions could help to rigidify the molecular conformation and lock the molecular rotations of the G-phase, resisting the effect from the external pressure, thereby showing a lower sensitivity to the pressure. In contrast, owing to the lack of C-H...N interactions, the O-phase could sensitively respond to the external hydrostatic pressure with a higher sensitivity.

Density functional theory (DFT) calculations by using the CASTEP module in Material Studio were performed on the basis of the structural data of a single crystal, for further investigating the change in the molecular geometry and packing structure under external pressure.^{6h} The optimized lattice parameters and geometrical parameters under the external stresses of 0, 1, 2 and 3 GPa were obtained and listed in Tables S7–S10 (ESI†). As the parameters show, the molecular geometries trended toward the planarization conformation and the molecular packing became tighter with the increase in the external stress. It was noted that the change in the molecular geometry and the molecular packing was bigger in the O-phase, according to the lattice parameters and roll angles, which was in accordance with the fewer varieties of intermolecular interactions in the O-phase, contributing to a higher sensitivity of the O-phase to the pressure.

Protonation–deprotonation effect

The protonation–deprotonation effect of the two crystalline phases was investigated. As shown in Fig. 5a, the fumigation with HCl vapor had a significant effect on the luminescence of the G-phase, turning it from green (511 nm) to red (610 nm), while the O-phase showed a weak luminescence switching from 575 to 595 nm. The acidified G-phase turned to green emission (blue-shifting from 610 to 530 nm) by fuming with diethylamine

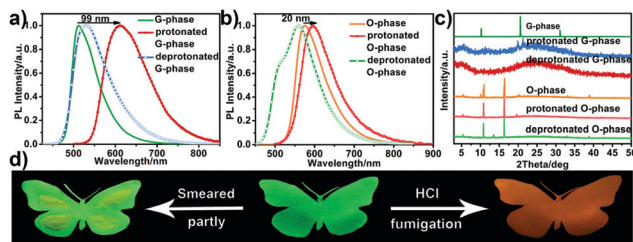


Fig. 5 (a and b) PL spectra of the initial two crystalline phases under different stimuli. (c) PXRD patterns of the initial two crystalline phases under different stimuli. (d) The butterfly patterns smeared partly and fumed by HCl vapor.

(DEA). The acidified O-phase also showed green emission (shifting from 595 to 559 nm) and a shoulder peak at 517 nm by treating with DEA vapor. PXRD analysis (Fig. 5c) showed that after being fumed by HCl vapor for 2 min, all of the characteristic peaks of the G-phase vanished, and a new wide swell arose implying that the crystalline state of the initial phase was destroyed and turned to an amorphous state.^{6c} With the exposure to HCl vapor, the protons tended to attach to the exposed nitrogen in order to protonate the molecules. Meanwhile, incoming chloride ions were apt to form strong hydrogen bonds with the protonated molecules. Thus, the fluorescence emission of the protonated sample showed a red-shift. When being fumed by DEA vapor, protons were captured from the protonated pyridine by DEA vapor, and the two crystalline phases showed blue-shifted luminescent emission. But the amorphous state for the protonated G-phase could hardly be restored by the DEA vapor. As for the O-phase, the crystalline state was not destroyed under the protonation and deprotonation processes due to the different intermolecular interactions inside the two phases. In the crystal structure of the G-phase, the nitrogen atom of a pyridine group could form strong C–H···N interactions with the adjacent molecules which would be broken by the incoming HCl due to the protonation of the nitrogen atom of the pyridine group, resulting in the destruction of the crystalline phase. Conversely, there were no C–H···N interactions in the O-phase, thus, the initial intermolecular interactions were not destroyed by protonating and deprotonating, as proved by the intense diffraction patterns. And the more hypsochromic luminescent emission with a weak shoulder peak of the alkalinized O-phase might be attributed to a faint change from the molecular conformation on the surface of crystals under the successive stimuli of acid and alkali.

In order to understand the acidochromism in depth, single crystals of protonated **BP3SA** (C–HCl Fig. S6a, ESI[†]) were obtained by using the solvent evaporation method. When a droplet of HCl was added in a mixed **BP3SA** solution of dichloromethane and methanol (volume ratio = 2 : 1), protonated crystals C–HCl can be obtained and show orange luminescent emission at 580 nm (Fig. S7, ESI[†]). X-ray structural analysis revealed that the molecular crystals were in the symmetrical protonation states, with abundant strong multiple X–H···Cl[−] (X = O, N) and C–H···π interactions in C–HCl crystals (for detailed data see Fig. S6 and Table S4, ESI[†]), which was consistent with the analysis of the protonated crystals. Furthermore, the PXRD pattern of C–HCl was not consistent with those of the protonated

crystals (Fig. S8, ESI[†]). Thus, the original crystals could not transfer to C–HCl by protonation. To gain further understanding of the relationship between the fluorescence change in the protonation process, density functional theory calculations were performed for C–HCl (Fig. S9, ESI[†]). Since the protonation of nitrogen atoms could greatly enhance the electron-withdrawing ability of pyridyl,^{11a,18} the electron cloud of the LUMO spreads on the pyridine group compared to those of the G-phase and O-phase. Thus, the C–HCl molecule had a smaller band gap 1.18 eV, which was compatible with the observed red-shifted emission of the G-phase and O-phase after the protonation.

To explore the application of materials, we carried out multiple external treatments on a butterfly-shape filter paper which was processed in a fluorescent dye solution. As shown in Fig. 5d, the original empty pattern was transferred into the vivid one by partly smearing, and after fuming with HCl vapor, the colour of the butterfly obviously changed from green to orange red. The results indicated that this kind of material had practical applications in high security inks.

Conclusions

In summary, we have demonstrated remarkable luminescence switching upon grinding force, hydrostatic pressure, and acid and alkali treatments based on two polymorphs of the novel molecule **BP3SA**. The G-phase with J-type aggregation shows green emission, while the O-phase with H-type aggregation presents orange emission. Upon grinding, the change in the aggregation states results in the red-shifts in luminescence of the two polymorphs. Upon further heating, the ground samples can partly recover their initial emissive colours. In addition, a structural transition from the O-phase to the G-phase appears during grinding and further heating processes. According to high-pressure experiments and theoretical calculations, fewer various intermolecular interactions are beneficial for higher sensitivity to the hydrostatic pressure. The protonation–deprotonation of the two polymorphs indicates that fumigation with HCl/DEA vapor leads to the destruction and reconstruction of the noncovalent C–H···N bonds, resulting in more distinct luminescence switching in the G-phase than the O-phase. This study on **BP3SA** provides comprehensive insight into the relationship between crystal structures and stimuli responsive properties, and further opens up an avenue for obtaining OMSRL materials.

Conflicts of interest

There are no conflicts to declare.

Acknowledgements

This work was supported by the Natural Science Foundation of China (21835001, 51773080, 21674041, 51573068, and 21221063), Program for Changbaishan Scholars of Jilin Province, Jilin Province project (20160101305JC), and the “Talents Cultivation Program” of Jilin University.

Notes and references

- 1 (a) H. Yanagi, T. Ohara and T. Morikawa, *Adv. Mater.*, 2001, **13**, 1452; (b) M. B. Pierre, M. A. Chad and R. R. John, *Acc. Chem. Res.*, 2010, **43**, 1396; (c) A. L. Balch, *Angew. Chem., Int. Ed.*, 2009, **48**, 2641; (d) K. Ariga, T. Mori and J. P. Hill, *Adv. Mater.*, 2012, **24**, 158; (e) F. Ciardelli, G. Ruggeri and A. Pucci, *Chem. Soc. Rev.*, 2013, **42**, 857; (f) E. P. Chan, J. J. Walsh, A. M. Urbas and E. L. Thomas, *Adv. Mater.*, 2013, **25**, 3934; (g) C. Jobbágy and A. Deák, *Eur. J. Inorg. Chem.*, 2014, 4434; (h) Y. Sagara, S. Yamane, M. Mitani, C. Weder and T. Kato, *Adv. Mater.*, 2016, **28**, 1073; (i) Z. Y. Ma, Z. J. Wang, M. J. Teng, Z. J. Xu and X. R. Jia, *ChemPhysChem*, 2015, **16**, 1811; (j) T. Seki and H. Ito, *Chem. – Eur. J.*, 2016, **22**, 4322.
- 2 (a) X. Zhang, N. Y. Xu, Q. Ruan, D. Q. Lu, Y. H. Yang and R. Hu, *RSC Adv.*, 2018, **8**, 5714; (b) W. Li, P.-P. Yang, L. Wang and H. Wang, *J. Mater. Chem. C*, 2015, **3**, 3783; (c) A. Pucci, R. Bizzarri and G. Ruggeri, *Soft Matter*, 2011, **7**, 3689; (d) A. Pucci and G. Ruggeri, *J. Mater. Chem.*, 2011, **21**, 8282.
- 3 (a) Z. L. Xie, Q. Y. Huang, T. Yu, L. Y. Wang, Z. Mao, W. L. Li, Z. Yang, Y. Zhang, S. W. Liu, J. R. Xu, Z. G. Chi and M. P. Aldred, *Adv. Funct. Mater.*, 2017, **27**, 1; (b) R. Pashazadeh, P. Pander, A. Lazauskas, F. B. Dias and J. V. Grazulevicius, *J. Phys. Chem. Lett.*, 2018, **9**, 1172; (c) H. J. Kim, D. R. Whang, J. Gierschner, C. H. Lee and S. Y. Park, *Angew. Chem., Int. Ed.*, 2015, **54**, 4330; (d) Y. Sagara and T. Kato, *Nat. Chem.*, 2009, **1**, 605.
- 4 Q. K. Qi, Y. F. Liu, X. F. Fang, Y. M. Zhang, P. Chen, Y. Wang, B. Yang, B. Xu, W. J. Tian and S. X. A. Zhang, *RSC Adv.*, 2013, **3**, 7996.
- 5 (a) L. Wang, K. Wang, B. Zou, K. Q. Ye, H. Y. Zhang and Y. Wang, *Adv. Mater.*, 2015, **27**, 2918; (b) Y. J. Dong, S. P. Wen, B. Li, L. Ye, B. Zou and W. J. Tian, *Angew. Chem., Int. Ed.*, 2012, **51**, 10782; (c) D. P. Yan and D. G. Evans, *Mater. Horiz.*, 2014, **1**, 46; (d) D. P. Yan, H. J. Yang, Q. Y. Meng, H. Y. Lin and M. Wei, *Adv. Funct. Mater.*, 2014, **24**, 587.
- 6 (a) A. Ekbote, S. M. Mobin and R. J. Misra, *J. Mater. Chem. C*, 2018, **6**, 10888; (b) H. Wang, W. J. Wang, J. P. Guan, M. S. Yuan and J. Y. Wang, *J. Lumin.*, 2017, **192**, 925; (c) J. B. Xiong, K. Wang, Z. Q. Yao, B. Zou, J. L. Xu and X. H. Bu, *ACS Appl. Mater. Interfaces*, 2018, **10**, 5819; (d) T. Jadhav, B. Dhokale, Y. Patil, S. M. Mobin and R. Misra, *J. Phys. Chem. C*, 2016, **120**, 24030; (e) Z. Gao, K. Wang, F. M. Liu, C. F. Feng, X. He, J. Y. Li, B. Yang, B. Zou and P. Lu, *Chem. – Eur. J.*, 2017, **23**, 773; (f) J. X. Wu, J. Tang, H. L. Wang, Q. K. Qi, X. F. Fang, Y. F. Liu, S. Q. Xu, S. X. A. Zhang, H. Y. Zhang and W. Q. Xu, *J. Phys. Chem. A*, 2015, **119**, 9218; (g) H. S. Yuan, K. Wang, K. Yang, B. B. Liu and B. Zou, *J. Phys. Chem. Lett.*, 2014, **5**, 2968; (h) Q. K. Qi, J. Y. Qian, X. Tan, J. B. Zhang, L. J. Wang, B. Xu, B. Zou and W. J. Tian, *Adv. Funct. Mater.*, 2015, **25**, 4005.
- 7 (a) Y. J. Dong, J. B. Zhang, X. Tan, L. J. Wang, J. L. Chen, B. Li, L. Ye, B. Xu, B. Zou and W. J. Tian, *J. Mater. Chem. C*, 2013, **1**, 7554; (b) Y. J. Liu, Q. X. Zeng, B. Zou, Y. Liu, B. Xu and W. J. Tian, *Angew. Chem., Int. Ed.*, 2018, **57**, 15670.
- 8 (a) Y. J. Zhang, K. Wang, G. L. Zhuang, Z. Q. Xie, C. Zhang, F. Cao, G. X. Pan, H. F. Chen, B. Zou and Y. G. Ma, *Chem. – Eur. J.*, 2015, **21**, 2474; (b) S. T. Zhang, Y. X. Dai, S. Y. Luo, Y. Gao, N. Gao, K. Wang, B. Zou, B. Yang and Y. G. Ma, *Adv. Funct. Mater.*, 2017, **27**, 7.
- 9 (a) L. Wang, K. Wang, H. Y. Zhang, C. J. Jiao, B. Zou, K. Q. Ye, H. Y. Zhang and Y. Wang, *Chem. Commun.*, 2015, **51**, 7701; (b) X. Q. Wang, Q. S. Liu, H. Yan, Z. P. Liu, M. G. Yao, Q. F. Zhang, S. W. Gong and W. J. He, *Chem. Commun.*, 2015, **51**, 7497.
- 10 (a) Y. X. Xu, K. Wang, Y. J. Zhang, Z. Q. Xie, B. Zou and Y. G. Ma, *J. Mater. Chem. C*, 2016, **4**, 1257; (b) W. Li, Y. M. Zhang, T. Zhang, W. R. Zhang, M. J. Li and S. X. A. Zhang, *J. Mater. Chem. C*, 2016, **4**, 1527; (c) Y. Li, Z. Y. Ma, A. S. Li, W. Q. Xu, Y. C. Wang, H. Jiang, K. Wang, Y. S. Zhao and X. R. Ji, *ACS Appl. Mater. Interfaces*, 2017, **9**, 8910; (d) R. R. Cui, Y. C. Lv, Y. S. Zhao, N. Zhao and N. Li, *Mater. Chem. Front.*, 2018, **2**, 910; (e) X. Meng, G. Y. Qi, X. Li, Z. Y. Wang, K. Wang, B. Zou and Y. G. Ma, *J. Mater. Chem. C*, 2016, **4**, 7584; (f) W. Z. Cai, R. Zhang and Y. S. Yao, *Phys. Chem. Chem. Phys.*, 2017, **19**, 6216; (g) Y. X. Dai, S. T. Zhang, H. C. Liu, K. Wang, F. F. Li, B. Han, B. Yang and B. Zou, *J. Phys. Chem. C*, 2017, **121**, 4909; (h) C. Weder, *J. Mater. Chem.*, 2011, **21**, 8235; (i) Z. G. Chi, X. Q. Zhang, B. J. Xu, X. Zhou, C. P. Ma, Y. Zhang, S. W. Liu and J. R. Xu, *Chem. Soc. Rev.*, 2012, **41**, 3878; (j) X. Q. Zhang, Z. G. Chi, Y. Zhang, S. W. Liu and J. R. Xu, *J. Mater. Chem. C*, 2013, **1**, 3376.
- 11 (a) S. Q. Ma, J. B. Zhang, Y. J. Liu, J. Y. Qian, B. Xu and W. J. Tian, *J. Phys. Chem. Lett.*, 2017, **8**, 3068; (b) J. B. Zhang, J. L. Chen, B. Xu, L. J. Wang, S. Q. Ma, Y. J. Dong, B. Li, L. Ye and W. J. Tian, *Chem. Commun.*, 2013, **49**, 3878; (c) A. K. Srivastava, A. K. Singh, N. Kumari, R. Yadav, A. Gulino, A. Speghini, R. Nagarajan and L. Mishra, *J. Lumin.*, 2017, **182**, 274.
- 12 (a) M. W. Li, Y. Yuan and Y. L. Chen, *ACS Appl. Mater. Interfaces*, 2018, **10**, 1237; (b) S. Achelle, J. Rodríguez-López, C. Katan and F. R. Guen, *J. Phys. Chem. C*, 2016, **120**, 26986; (c) D. Liu, Z. Zhang, H. Zhang and Y. Wang, *Chem. Commun.*, 2013, **49**, 10001.
- 13 J. L. Chen, S. Q. Ma, J. B. Zhang, L. J. Wang, L. Ye, B. Li, B. Xu and W. J. Tian, *J. Phys. Chem. Lett.*, 2014, **5**, 2781.
- 14 (a) P. J. Pacheco-Liñán, J. Fernández-Sainz, I. Bravo, A. Garzón-Ruiz, C. Alonso-Moreno, F. Carrillo-Hermosilla, A. Antiñolo and J. Albaladejo, *J. Phys. Chem. C*, 2018, **122**, 9363; (b) P. C. Xue, B. Q. Yao, Y. B. Shen and H. Q. Gao, *J. Mater. Chem. C*, 2017, **5**, 11496; (c) S. J. Chen, W. Liu, Z. H. Ge, W. X. Zhang, K. P. Wang and Z. Q. Hu, *CrystEngComm*, 2018, **20**, 5432; (d) E. L. Spitzer and M. M. Haley, *Tetrahedron*, 2008, **64**, 11469; (e) B. Lu, Y. J. Zhang, X. G. Yang, K. Wang, B. Zou and D. P. Yan, *J. Mater. Chem. C*, 2018, **6**, 9660.
- 15 S. Varghese, S. K. Park, S. Casado, R. C. Fischer, R. Resel, B. M. Medina, R. Wannemacher, S. Y. Park and J. Gierschner, *J. Phys. Chem. Lett.*, 2013, **4**, 1597.
- 16 (a) M. S. Kwon, J. Gierschner, S. J. Yoon and S. Y. Park, *Adv. Mater.*, 2012, **24**, 5487; (b) W. Yang, C. L. Liu, S. Lu, J. Y. Du, Q. Y. Gao, R. H. Zhang, Y. Liu and C. Y. Yang, *J. Mater. Chem. C*, 2018, **6**, 290.
- 17 K. Nagura, S. Saito, H. Yusa, H. Yamawaki, H. Fujihisa, H. Sato, Y. Shimoikeda and S. Yamaguchi, *J. Am. Chem. Soc.*, 2013, **135**, 10322.
- 18 P. Xue, B. Yao, P. Wang, J. Sun, Z. Zhang and R. Lu, *RSC Adv.*, 2014, **4**, 58732.